

# Observation of Strong Terahertz Radiation from a Liquid Water Line

L.-L. Zhang,<sup>1</sup> W.-M. Wang,<sup>2,1,3,\*</sup> T. Wu,<sup>4</sup> S.-J. Feng,<sup>4</sup> K. Kang,<sup>1</sup> C.-L. Zhang,<sup>1</sup> Y. Zhang,<sup>1</sup> Y.-T. Li,<sup>2,3</sup> Z.-M. Sheng,<sup>5,6,7,8</sup> and X.-C. Zhang<sup>9,1</sup>

<sup>1</sup>*Beijing Advanced Innovation Center for Imaging Technology  
and Key Laboratory of Terahertz Optoelectronics (MoE),  
Department of Physics, Capital Normal University, Beijing 100048, China*

<sup>2</sup>*Beijing National Laboratory for Condensed Matter Physics,  
Institute of Physics, CAS, Beijing 100190, China*

<sup>3</sup>*Songshan Lake Materials Laboratory,  
Dongguan, Guangdong 523808, China*

<sup>4</sup>*Beijing Key Laboratory for Precision Optoelectronic Measurement  
Instrument and Technology, School of Optoelectronics,  
Beijing Institute of Technology, Beijing 100081, China*

<sup>5</sup>*SUPA, Department of Physics, University of Strathclyde,  
Glasgow G4 0NG, United Kingdom*

<sup>6</sup>*Key Laboratory for Laser Plasmas (MoE) and School of Physics and Astronomy,  
Shanghai Jiao Tong University, Shanghai 200240, China*

<sup>7</sup>*IFSA Collaborative Innovation Center,  
Shanghai Jiao Tong University, Shanghai 200240, China*

<sup>8</sup>*Tsung-Dao Lee Institute, Shanghai Jiao Tong University, Shanghai 200240, China*

<sup>9</sup>*The Institute of Optics, University of Rochester, Rochester, New York 14627, USA*

(Dated: December 27, 2018)

## Abstract

Terahertz radiation generation from liquid water has long been considered to be impossible due to strong absorption. A few very recent works reported terahertz generation from water, but the mechanism is not clear and the efficiency demands to be enhanced. We show experimentally that strong single-cycle terahertz radiation with field strength of  $0.2 \text{ MVcm}^{-1}$  is generated from a water line/column of  $\sim 200\mu\text{m}$  in diameter irradiated by a mJ femtosecond laser beam. This strength is 100-fold higher than that produced from air. We attribute the mechanism to the laser-ponderomotive-force-induced current with the symmetry broken around the water-column interface. This mechanism can explain our following observations: the radiation can be generated only when the laser propagation axis deviates from the column center; the deviation determines its field strength and polarity; it is always p-polarized no matter whether the laser is p- or s-polarized. This study provides a simple and efficient scheme of table-top terahertz sources based on liquid water.

PACS numbers: 42.65.Re, 32.80.Fb, 52.38.-r, 52.65.Rr

Achieving table-top terahertz (THz) sources with high field strength and broad bandwidth is an outstanding issue in THz science. Such sources can find applications in material research [1, 2], biomedical imaging [3], non-destructive detection [4], and THz-field matter interactions [5, 6]. Previous studies have demonstrated THz generation from solids [8–11] and gases [12–22] via different mechanisms. However, THz generation from liquid, in particular water, has long been considered impossible because of its strong absorption of THz radiation. On the other hand, water exists in most biological systems and hence THz radiation generated from liquid water may carry some information of these systems. Therefore, how to generate THz radiation from water is fundamental challenge for both basic and applied research. In 2017, two groups reported THz emission from liquid water [23, 24]. When an intense laser beam of tens of mJ was focused on liquid water in a cuvette, extreme broadband THz radiation was generated [23], where it is considered that laser spectral broadening played a key role. In the other work [24], when a mJ laser beam irradiated a water film with the thickness  $\sim 200 \mu\text{m}$ , THz radiation was produced with 1.8 times higher strength than that produced from air. So far, the THz radiation mechanism in water has not yet been well clarified and the yield efficiency demands to be further enhanced.

Here, we demonstrate experimentally that the efficiency can be enhanced by three orders of magnitude when a water column with the diameter  $\sim 200 \mu\text{m}$  is adopted. With a mJ femtosecond laser beam, the THz field strength can reach  $0.2 \text{ MVcm}^{-1}$  which is as high as generated via the standard two-color laser scheme in air [12, 13]. To explain our result, we propose that the THz radiation originates from a net current formed due to the presence of the column interface. The laser self-focusing in water causes a plasma to be produced. The laser ponderomotive force forms positive and negative currents distributed on two sides of the laser propagation axis, respectively. The symmetry of the two currents can be broken provided the laser axis deviates from the water column center. As the deviation grows, the net current and resulting THz radiation will be strengthened. This mechanism implies that the THz polarization is on the column cross-section plane and its strength scales linearly with the laser energy. These are verified by our experiments and particle-in-cell (PIC) simulations.

*Experimental setup.*— Figure 1 shows a schematic of our experiment, where a laser beam is incident along the  $+z$  direction and the water column axis is along the  $y$  direction. The laser beam is delivered from a Ti:Sapphire amplifier (Spitfire, Spectra Physics) with a central

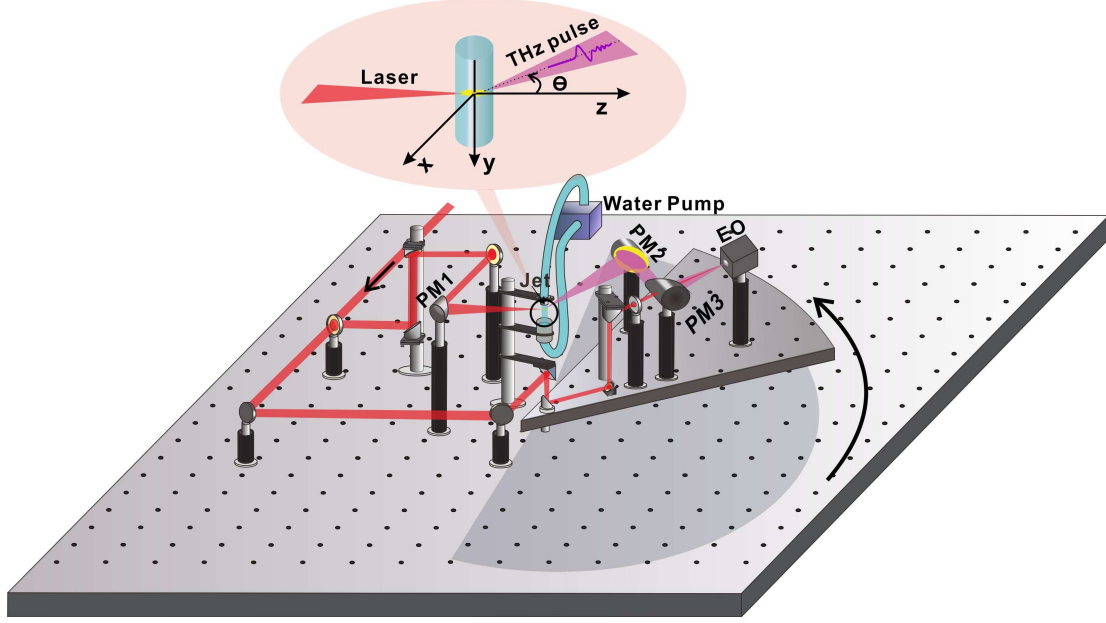


FIG. 1. Experimental setup, where PM1-3 are parabolic mirrors and EO is electro-optical detection. The inset illustrates the geometry of the laser interaction with the water column, where THz pulses can be detected at an angle  $\theta$  rotating from the laser axis ( $z$ ) in the incident plane  $xoz$ .

wavelength 800nm, pulse duration 100fs, and repetition rate 1kHz. It is split into pump and probe beams with controllable time delay. The pump beam is focused by an off-axis parabolic mirror (PM1) with 1-inch equivalent focal length. The polarization of the pump beam is linear and its orientation can be rotated through a half-wave plate. A liquid geyser with a pressure of 0.1MPa creates a free-flowing water column with the diameter  $\sim 200 \mu\text{m}$  near the tip of the geyser. The water column is located around the focusing plane of the pump beam and can precisely move along the  $x$  direction (equivalent to the shift of the laser propagation axis). Here, we fix the coordinate on the column and set the column center as the origin, as shown in the inset.

The THz pulse is collimated and refocused by two parabolic mirrors. Filters are placed in the THz path to block the residual laser beam. The probe laser beam passes through a pair of climbing mirrors, is focused by a 125mm convex lens, and co-propagates with the THz pulse which has passed through a hole drilled on the back of the parabolic mirror (PM3). The collection portion is installed on a platform which can be rotated around the water column to detect the THz pulse at an angle  $\theta$  (positive: anti-clockwise) with respect to the laser incident direction. To reduce the user intervention and the experimental error, we

minimize the optical path difference between the pump and probe beam arms of rotation. The THz fields resolved traces are obtained through electro-optic (EO) sampling with a 3 mm thick  $\langle 110 \rangle$ -cut ZnTe crystal as the detector [25]. In our experiments, the laser beam is taken as 2 mJ energy, p-polarization (along the  $x$  direction), the laser propagation axis is displaced  $60 \mu\text{m}$  ( $x_L = 60 \mu\text{m}$ ) from the water column center, and the THz pulse is collected at  $\theta = 0^\circ$ , except in Fig. 4.

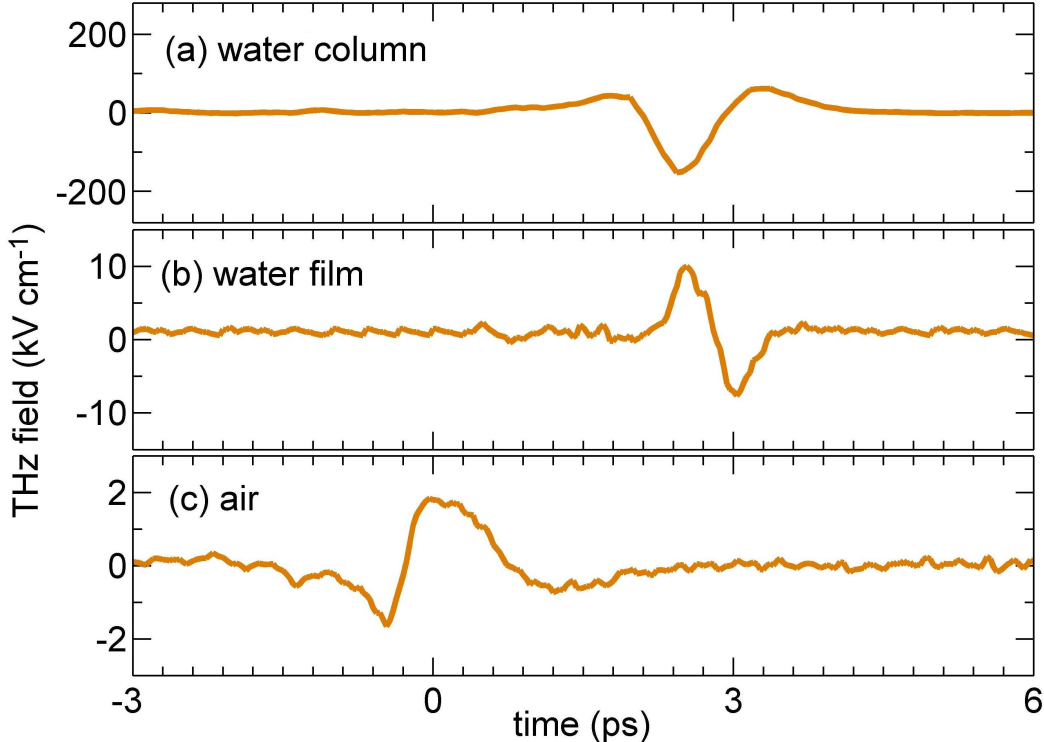


FIG. 2. THz pulses generated from (a) water column with the normal laser incidence and  $x_L = 60 \mu\text{m}$ , (b) water film with the laser incident angle of  $60^\circ$ , and (c) air with the normal laser incidence. The THz pulses are detected by electro-optic sampling and collected at  $\theta = 0^\circ$ .

*Demonstration of THz generation.*— Figure 2(a) shows the waveform of the THz pulse generated from the water column. As comparison, the ones from water film and air irradiated by the same laser beam are also displayed in Figs. 2(b) and 2(c). The THz pulse from the water column has a field strength about  $0.2 \text{ MVcm}^{-1}$ , 20-fold and 100-fold higher than the one from the water film and air, respectively. The THz strength is as high as the one with the standard two-color laser scheme in air [12, 13] even though a one-color laser beam is used here. Note that the strength can be further enhanced when the THz pulse is collected at  $\theta$  of  $40^\circ - 60^\circ$  rather than  $\theta = 0^\circ$  [this will be shown in Fig. 4(c)]. In Fig. 2(b) we

take a 200- $\mu\text{m}$ -thick and 5-mm-wide water film, which is produced by a jet nozzle with polished sapphire surfaces (Sirah, Germany). The laser incident angle is taken as  $60^\circ$  to optimize the THz strength, in particular, nearly no THz generation with the laser normal incidence [24]. However, in the water column case, the normal laser incidence along the  $+z$  direction is always taken in our experiments and efficient THz generation is observed (note that the laser beam with a self-focusing intensity  $\sim 10^{15} \text{ Wcm}^{-2}$  ionizes the water column to be plasma and then the beam can propagate along its incident direction since the plasma refractive index approaches 1 in our case). This suggests that there are different generation mechanisms in the two cases [different THz strength scaling are also observed as shown in Fig. 4(a)]. Here, we focus on the water column case and exploration of the mechanism in the water film is beyond the scope of this work.

*Mechanism.*— The experimental and PIC-simulation results shown in Fig. 3 suggest that the mechanism can be explained as the laser-ponderomotive-force-induced current with the symmetry broken around the column interface. Figure 3(a) shows that the THz pulses have nearly the same amplitude and opposite field signs when the laser axis deviates from the column center by  $+60\mu\text{m}$  and  $-60\mu\text{m}$  ( $x_L = \pm 60\mu\text{m}$ ), respectively. While the laser axis is at the column center ( $x_L = 0$ ), virtually no THz pulse is generated, as seen in Fig. 3(b). This figure also shows that the THz strengths have the same absolute value and opposite signs at the two points  $\pm x_L$ . As  $|x_L|$  is increased, the amplitude is first enhanced and then lowered. The amplitude peaks appear around  $x_L = \pm(60\mu\text{m} \sim 70\mu\text{m})$ . These are in agreement with our PIC simulation results shown by the line in Fig. 3(b), which are explained below.

Our simulations are performed with the KLAPS code [26], in which we adopt the same parameters of the water column and laser (energy, duration, and polarization) as in the experiments. Considering that the laser self-focusing in water should be stronger than in air, we assume that the laser beam in the water column has the spot radius  $w_0 = 30 \mu\text{m}$ . Then, the corresponding intensity is  $1.5 \times 10^{14} \text{ Wcm}^{-2} - 1.7 \times 10^{15} \text{ Wcm}^{-2}$  when the laser energy varies within 0.2 mJ – 2.4 mJ. In our simulations, the laser energy is taken as 2mJ ( $1.2 \times 10^{15} \text{ Wcm}^{-2}$ ) except Fig. 4(a). With such laser intensity, plasma is quickly produced by the laser beam via field ionization. No net current can be formed via the ionization since the symmetry of the ionization by a one-color 800nm laser beam is not broken [17, 27].

On the other hand, our simulations show in Fig. 3(c) that net currents can be formed in the laser interactions with the water-column plasma. We examine the quasi-static currents

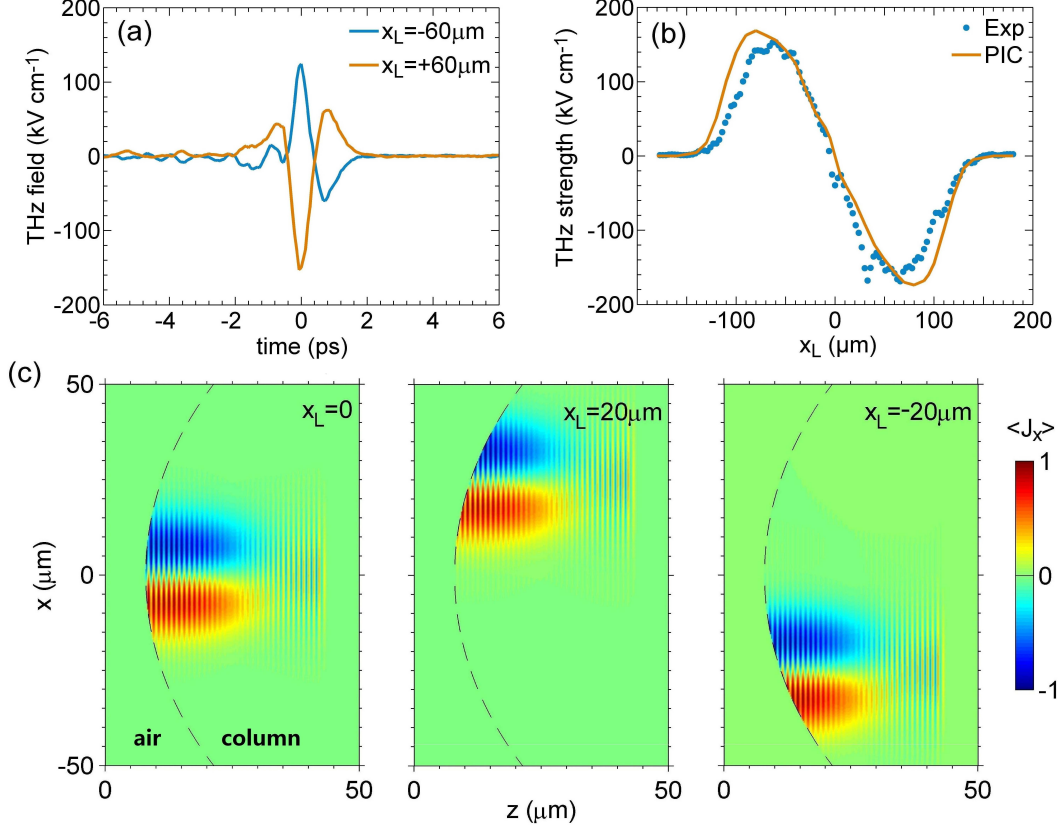


FIG. 3. (a) THz pulses observed in the experimenters with  $x_L = \pm 60 \mu m$ . (b) THz strength as a function of  $x_L$ , where experimental and PIC results are shown by dots and line, respectively. (c) PIC results of quasi-static currents  $\langle J_x \rangle$  with different  $x_L$ , where the currents are obtained by temporally averaging  $J_x$  over one laser cycle and the broken line in each plots marks the column interface.

$\langle J_x \rangle$ ,  $\langle J_y \rangle$ , and  $\langle J_z \rangle$ , respectively, where these currents are obtained by temporally averaging  $J_x$ ,  $J_y$ , and  $J_z$  over one laser cycle. Here, the laser polarization is along the  $x$  direction (p-polarization). One can see in Fig. 3(c) that the total/net currents  $\sum \langle J_x \rangle \neq 0$  unless  $x_L = 0$ , where  $\sum$  means spatial summation. When  $x_L = 0$ , the positive and negative currents are symmetrically distributed, therefore, the net current is zero. When  $x_L = 20 \mu m$ , the positive current is distributed within a larger area than the negative one, therefore, the net current is positive. While  $x_L = -20 \mu m$ , the positive current is distributed within a smaller area, therefore, the net current is negative. In addition, the net currents  $\sum \langle J_y \rangle$  and  $\sum \langle J_z \rangle$  remain zero with any  $x_L$ , as in usual cases without special target interfaces.

The net current is formed in the  $x$  direction because of the column interface in the laser

incident plane as well as the spatial non-uniform of laser intensity. With a Gaussian laser beam, the laser ponderomotive force [28] pushes the plasma electrons away from the laser axis. Hence, the quasi-static current is negative on the upper ( $x > x_L$ ) and positive on the lower ( $x < x_L$ ). Around the column interface, the electrons pushed by the ponderomotive force are pulled back by the plasma ions due to strong charge-separation fields. This prevents the electrons from escaping away from the interface, constraining the current near the interface. Hence, the interface breaks the symmetry between the positive and negative currents. The area difference between the positive and negative currents can be estimated with

$$\Delta S = 2f(x_L) - f(x_L + w) - f(x_L - w), \quad (1)$$

where  $f(x) = [x\sqrt{R^2 - x^2} + R^2 \arcsin(x/R)]/2$ ,  $R$  is the column radius and  $w$  is the efficient width of the laser beam ( $w$  at the order of  $w_0$ ). Obviously,  $|\Delta S|$  grows with increasing  $|x_L|$ . Provided  $x_L$  is replaced by  $-x_L$ , the absolute value of  $\Delta S$  remains constant, but its sign is reversed. This can explain the experimental and PIC results within  $|x_L| < x_L^{opt}$  shown in Fig. 3(b) (THz peaks at  $\pm x_L^{opt}$ ), since  $J_{net} \propto \Delta S$  and  $E_{THz} \propto J_{net}$  [18, 22]. Note that in Figs. 3(b),4(a),4(b) we present the net-current strengths obtained from our PIC simulations. Similar to the two-color scheme in air [17, 19], THz pulses can be generated once net currents are formed in plasma due to the plasma modulation [18], which causes single-cycle waveforms of the THz pulses [see Figs. 2(a),3(a)]. Note that we have discussed  $\Delta S$  in the laser-entrance side, which can directly be applied in the laser-exit side since the laser beam is normally incident and the water plasma density is low.

Figure 3(b) also shows that there are optimized values of  $x_L$  for the THz field strength. This is because the zone of laser-water and laser-plasma interactions becomes too small if  $|x_L|$  is taken as a large value, which limits the THz generation. According to our PIC simulations,  $x_L^{opt}$  depends on the laser spot radius  $w_0$ :  $x_L^{opt} \simeq 92\mu m$  with  $w_0 = 15\mu m$ ,  $x_L^{opt} \simeq 80\mu m$  with  $w_0 = 30\mu m$  [see Fig. 3(b)], and  $x_L^{opt} \simeq 70\mu m$  with  $w_0 = 45\mu m$ . Based on the simulation results, we could roughly summarize as  $x_L^{opt} \simeq R - 2w_0/3$ . This value varies slightly with the laser energy within the range of 0.2mJ to 2.4mJ.

*THz strength scaling and polarization.*—The THz field strength scaling with the laser intensity or energy is determined by the ponderomotive force. In a laser field, motion of an electron is governed by the Hamiltonian  $H = mc^2\gamma - e\varphi$ , where  $\mathbf{p}$  and  $\gamma = \sqrt{1 + (\mathbf{p}/mc)^2}$



are the momentum and relativistic factor, respectively,  $e$  and  $m$  are the electron charge and mass, respectively,  $c$  is the light speed in vacuum, and  $\varphi$  is the scalar potential generated due to the plasma response. Taking the spatial derivative of  $H$ , one can obtain  $dp_z/dt = \partial(e\varphi - mc^2\gamma)/\partial z$  and  $d(\mathbf{p}_\perp - e\mathbf{A}/c)/dt = \nabla_\perp(e\varphi - mc^2\gamma)$ , where  $\mathbf{A}$  is the laser vector potential. We consider a plasma with the plasma oscillating frequency  $\omega_p = \sqrt{4\pi e^2 n_e/m}$  much lower than the laser frequency  $\omega$ , where  $n_e$  is the plasma density. Note that the THz pulse frequency, which is roughly at  $\omega_p/2\pi$  [18, 22], is close to 1 THz according to Fig. 2(a). Therefore, it can be assumed that any physical quantity  $Q$  in this laser-plasma system can be divided into a fast varying part and a slowly varying part, i.e.,  $Q = Q^f + \langle Q \rangle$ , where  $Q^f$  varies at the order of  $\omega$ ,  $\langle Q \rangle$  at the order of  $\omega_p$ ,  $\langle Q \rangle = \int_0^T Q dt/T$ , and  $T = 2\pi/\omega$  is the laser cycle. The fast varying part of the momentum satisfies  $dp_z^f/dt = -mc^2\partial\gamma^f/\partial z$  and  $d(\mathbf{p}_\perp^f - e\mathbf{A}/c)/dt = 0$ . The slowly varying part satisfies  $d\langle \mathbf{p}_\perp \rangle/dt = e\nabla_\perp\varphi - mc^2\nabla_\perp\langle\gamma\rangle$ , where the first term on the right hand is the electrostatic force and the second is the ponderomotive force  $\mathbf{F}_p$ . In our case with  $\omega_p \ll \omega$ , basically  $|\langle \mathbf{p} \rangle| \ll |\mathbf{p}^f|$  and  $|e\nabla_\perp\varphi| \ll F_p$ . Therefore,  $\gamma \simeq 1 + e^2\mathbf{A}^2/2m^2c^4$  [29] and  $d\langle \mathbf{p}_\perp \rangle/dt \simeq \mathbf{F}_p = -e^2\nabla_\perp\langle\mathbf{A}^2\rangle/2mc^2$ . By applying  $\langle \mathbf{J}_\perp \rangle = -en_e\langle \mathbf{p}_\perp \rangle/m$  in a non-relativistic case, the quasi-static current induced by the ponderomotive force is given by

$$\left\langle \frac{\partial \mathbf{J}_\perp}{\partial t} \right\rangle \simeq \frac{e^3 n_e}{2m^2 c^2} \nabla_\perp \langle \mathbf{A}^2 \rangle. \quad (2)$$

This equation gives  $\langle \partial \mathbf{J}_\perp / \partial t \rangle \propto A_0^2/w_0^2 \propto \varepsilon_{laser}/w_0^2$ , where we consider a Gaussian beam with  $\nabla_\perp \langle \mathbf{A}^2 \rangle \sim A_0^2/w_0^2$  and the laser energy  $\varepsilon_{laser} \propto A_0^2$ . According to  $\mathbf{E}_{THz} \propto \langle \partial \mathbf{J}_\perp / \partial t \rangle$  [18, 22], one can obtain:

$$E_{THz} \propto \frac{\varepsilon_{laser}}{w_0^2}. \quad (3)$$

This linear scaling of the THz field strength with the laser energy is verified by our experimental and PIC results as shown in Fig. 4(a). Note that this scaling is different from that in the water film case [24], in which  $E_{THz} \propto \sqrt{\varepsilon_{laser}}$ . Equation (3) also suggests that the THz strength is decreased with the laser spot radius  $w_0$  in the water plasma. This is difficult to examine by experiments since  $w_0$  is mainly determined by the laser self-focusing in water. Our PIC simulation results roughly follow the scaling with  $1/w_0^2$ . For example, the net currents with  $w_0 = 15\mu m$  is 3-6 times (varying with  $x_L$ ) of those with  $w_0 = 30\mu m$  when the laser intensity is fixed. The deviation from the predicted value 4 could be explained as  $\Delta S$  also depends on  $w_0$  and  $x_L$ . Note that the plasma density  $n_e$  is nearly unchanged

when the laser energy is taken between 0.2mJ and 2.4mJ with the corresponding intensity  $2 \times 10^{14}$  W/cm –  $1.7 \times 10^{15}$  Wcm<sup>-2</sup>. In this intensity range, the first order of complete ionization occurs for both oxygen and hydrogen, but the second order of ionization of the oxygen can be ignored because it requires an intensity above  $2 \times 10^{15}$  Wcm<sup>-2</sup>.

The ponderomotive-induced current given in equation (2) is symmetric in any transverse direction, e.g., it is negative at  $y > 0$  and positive at  $y < 0$ , which exactly counteract each other. Hence, no net current can be formed in a transverse direction, except in the  $x$  direction. In this direction, the symmetry of the current can be broken by the water-column interface, as shown in Fig. 3(c). As a result, the THz polarization is always along the  $x$  direction (p-polarized), no matter whether the laser beam is taken as p-polarization or not. This is verified by our experiments, as shown in Fig. 4(b). We record the transverse components of the THz electric field by electro-optic sampling and then obtain the polarization trajectory by recomposing the THz fields. When we change the laser polarization angle from 0° (p-polarized) to 90° (s-polarized), the THz pulse keeps p-polarized (more results with different polarization angles are shown in Supplemental Material). These experimental results are reproduced by our PIC simulations.

Figure 4(c) shows the angular distribution of the THz pulses in the range of 0° – 90°. The THz pulses are stronger with  $x_L = -60\mu\text{m}$  than those with  $x_L = 60\mu\text{m}$ . This is because the detector is rotated with  $\theta > 0$  and located at  $x < 0$  (see Fig. 1), the THz pulses with  $x_L = 60\mu\text{m}$  need to pass through a longer distance of both water and plasma, hence, they are more strongly absorbed. With  $x_L = -60\mu\text{m}$  the peak angles appear around 40° – 60°. In this case, the pulses propagate mainly in the plasma towards the detector. Considering that the net current is along the  $x$  direction, the strongest emission from the current should be at  $\theta = 0^\circ$  and it weakens with increasing  $\theta$ . On the other hand, with  $\theta = 0^\circ$  the THz pulse propagates the longest distance in the plasma and it is most strongly absorbed and scattered by the plasma. The propagation distance and the absorption decreases with increasing  $\theta$ . The two factors cause the strongest THz pulses to be observed at 40° – 60°. These factors can also explain the energy decline from  $\theta = 0^\circ$  to 30° in the case with  $x_L = 60\mu\text{m}$ . However, paths of the pulses detected at larger  $\theta$  are difficult to obtained because they are affected by scattering and refraction at plasma-water and water-air boundaries and they significantly deviate from the initial emission direction. Finally, according to Fig. 4(c) we calculate the THz yield efficiency to be above  $6 \times 10^{-5}$ , which is as high as that with the two-color scheme

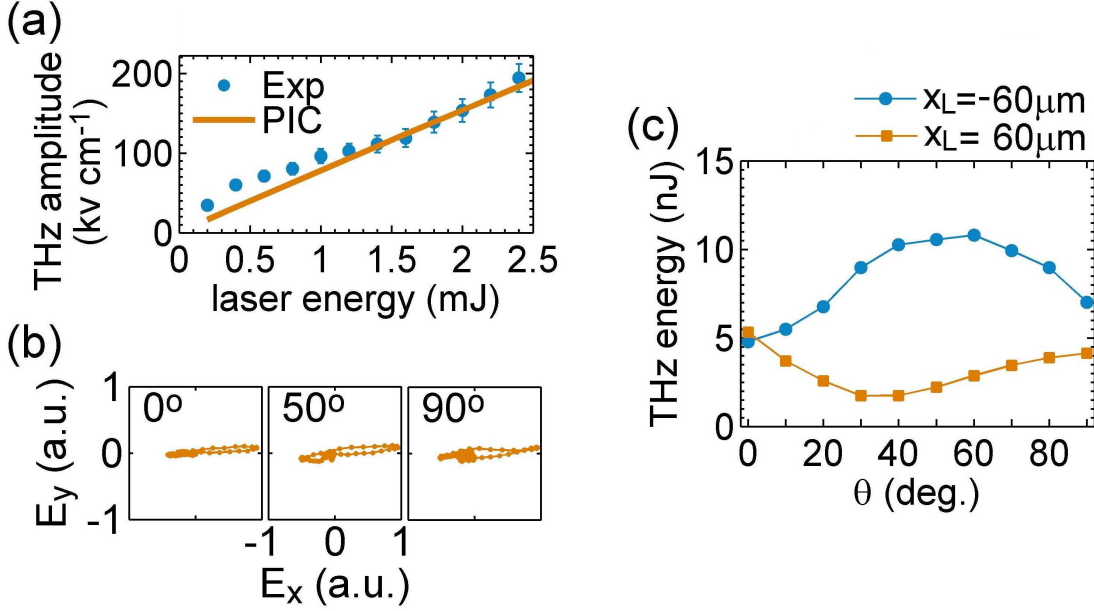


FIG. 4. (a) THz amplitude as a function of the laser energy, where experimental results are shown by dots and PIC results by the line. (b) Polarization trajectories of the  $x$  and  $y$  components of THz fields obtained experimentally, where three laser polarization angles  $0^\circ$ ,  $50^\circ$ , and  $90^\circ$  are taken, respectively. (c) The THz energy as a function of  $\theta$  observed in our experiments with  $x_L = \pm 60 \mu\text{m}$ , where the detector is located at  $x < 0$ .

pumped by 800nm lasers [20, 30].

In summary, we have proposed an efficient scheme to generate liquid-water-based THz radiation with a single laser beam, where the field strength and yield efficiency are as high as the standard two-color laser scheme in gases. Our experiments have shown that a water column irradiated by a 800 nm one-color laser beam of 2 mJ can emit broadband THz radiation with the strength of  $0.2 \text{ MVcm}^{-1}$ , two orders of magnitude higher than one from air or a water film. A laser-ponderomotive-force-induced current model has been proposed to explain the THz generation mechanism. The model predicts the dependence of the THz generation on laser energy, polarization, as well as the deviation between the laser axis and the column center, which has been verified by our experiments and PIC simulations. In particular, the THz field strength and even polarity can be controlled by the deviation.

This work was supported by National Key R&D Program of China (Grant No. 2018YFA0404801), National Natural Science Foundation of China (Grants No. 11775302 and 11721091), and Science Challenge Project of China (Grant No. TZ2016005). Z.-M. S. acknowledges the

support of a Leverhulme Trust Research Grant at the University of Strathclyde. X.-C. Z. was also partially sponsored by the Army Research Office and was accomplished under Grant No. US ARMY W911NF-17-1-0428. We thank Prof. David R. Jones for useful discussion.

---

\* e-mail: weiminwang1@126.com

- [1] B. Ferguson and X.-C Zhang, *Nat. Mater.* **1**, 26-33 (2002).
- [2] B. Clough, J. Dai, and X.-C. Zhang, *Mater. Today* **15**, 50 (2012).
- [3] D. Mittleman, *Sensing with Terahertz Radiation* (Springer-Verlag, 2003).
- [4] M. Tonouchi, *Nat. Photonics* **1**, 97-105 (2007).
- [5] T. Kampfrath, K. Tanaka, and K. Nelson, *Nat. Photonics* **7**, 680 (2013).
- [6] S. Spielman, B. Parks, J. Orenstein, D. T. Nemeth, F. Ludwig, J. Clarke, P. Merchant, and D. J. Lew, *Phys. Rev. Lett.* **73**, 1537 (1994).
- [7] F. Blanchard, G. Sharma, L. Razzari, X. Ropagnol, H.-C. Bandulet, F. Vidal, R. Morandotti, J.-C. Kieffer, T. Ozaki, and H. Tiedje, *IEEE J. Sel. Top. Quantum Electron.* **17**, 5 (2011).
- [8] Z. Jin, Z. L. Chen, H. B. Zhuo, A. Kon, M. Nakatsutsumi, H. B. Wang, B. H. Zhang, Y. Q. Gu, Y. C. Wu, B. Zhu, L. Wang, M. Y. Yu, Z. M. Sheng, and R. Kodama, *Phys. Rev. Lett.* **107**, 265003 (2011).
- [9] J. A. Fulop, L. Palfalvi, M. C. Hoffmann, and J. Hebling, *Opt. Express* **19**, 15090 (2011).
- [10] A. Gopal, S. Herzer, A. Schmidt, P. Singh, A. Reinhard, W. Ziegler, D. Brommel, A. Karmakar, P. Gibbon, U. Dillner et al., *Phys. Rev. Lett.* **111**, 074802 (2013).
- [11] G.-Q. Liao, Y.-T. Li, Y.-H. Zhang, H. Liu, X.-L. Ge, S. Yang, W.-Q. Wei, X.-H. Yuan, Y.-Q. Deng, B.-J. Zhu, Z. Zhang, W.-M. Wang, Z.-M. Sheng, L.-M. Chen, X. Lu, J.-L. Ma, X. Wang, and J. Zhang, *Phys. Rev. Lett.* **116**, 205003 (2016).
- [12] D. J. Cook and R. M. Hochstrasser, *Opt. Lett.* **25**, 1210 (2000).
- [13] M. Kress, T. Löffler, S. Eden, M. Thomson, and H. G. Roskos, *Opt. Lett.* **29**, 1120 (2004).
- [14] X. Xie, J. Dai, and X.-C. Zhang, *Phys. Rev. Lett.* **96**, 075005 (2006).
- [15] K. Y. Kim, A. J. Taylor, J. H. Glowina, and G. Rodriguez, *Nat. Photonics* **2**, 605 (2008).
- [16] H. C. Wu, J. Meyer-ter-Vehn, and Z. M. Sheng, *New J. Phys.* **10**, 043001 (2008).
- [17] K. Y. Kim, J. H. Glowina, A. J. Taylor and G. Rodriguez, *Opt. Express* **15**, 4577 (2007).

- [18] W.-M. Wang, Z.-M. Sheng, H.-C. Wu, M. Chen, C. Li, J. Zhang, and K. Mima, *Opt. Express* **16**, 16999 (2008).
- [19] I. Babushkin, W. Kuehn, C. Kohler, S. Skupin, L. Berge, K. Reimann, M. Woerner, J. Herrmann, and T. Elsaesser, *Phys. Rev. Lett.* **105**, 053903 (2010).
- [20] M. Clerici, M. Peccianti, B. E. Schmidt, L. Caspani, M. Shalaby, M. Giguere, A. Lotti, A. Couairon, F. Legare, T. Ozaki, D. Faccio, and R. Morandotti, *Phys. Rev. Lett.* **110**, 253901 (2013).
- [21] V. A. Andreeva, O. G. Kosareva, N. A. Panov, D. E. Shipilo, P. M. Solyankin, M. N. Esaulkov, P. Gonzalez de Alaiza Martinez, A. P. Shkurinov, V. A. Makarov, L. Berge, and S. L. Chin, *Phys. Rev. Lett.* **116**, 063902 (2016).
- [22] L.-L. Zhang, W.-M. Wang, T. Wu, R. Zhang, S.-J. Zhang, C.-L. Zhang, Y. Zhang, Z.-M. Sheng, and X.-C. Zhang, *Phys. Rev. Lett.* **119**, 235001 (2017).
- [23] I. Dey, K. Jana, V. Yu. Fedorov, A. D. Koulouklidis, A. Mondal, M. Shaikh, D. Sarkar, A. D. Lad, S. Tzortzakis, A. Couairon, G. R. Kumar, *Nat. Commun.* **8**, 1184 (2017).
- [24] Q. Jin, Y. E. K. Williams, J. Dai, and X.-C. Zhang, *Appl. Phys. Lett.* **111**, 071103 (2017).
- [25] Q. Wu and X.-C. Zhang, *Appl. Phys. Lett.* **67**, 3523 (1995).
- [26] W.-M. Wang, P. Gibbon, Z.-M. Sheng, and Y.-T. Li, *Phys. Rev. E* **91**, 013101 (2015).
- [27] W.-M. Wang, S. Kawata, Z.-M. Sheng, Y.-T. Li, J. Zhang, L. M. Chen, L. J. Qian, J. Zhang, *Opt. Lett.* **36**, 2608 (2011).
- [28] P. Gibbon, *Short Pulse Laser Interactions with Matter* (Imperial College Press, 2000).
- [29] W.-M. Wang, Z.-M. Sheng, Y.-T. Li, L.-M. Chen, S. Kawata, J. Zhang, *Phys. Rev. ST Accel. Beams* **13**, 071301 (2010).
- [30] T.-J. Wang, Y. Chen, C. Marceau, F. Theberge, M. Chateaufneuf, J. Dubois, and S. L. Chin, *Appl. Phys. Lett.* **95**, 131108 (2009).